

Article

# Self-Assembly and Electrical Conductivity of a New [1]benzothieno[3,2-b][1]-benzothiophene (BTBT)-Peptide Hydrogel

Anna Fortunato, Rafael Cintra Hensel, Stefano Casalini  and Miriam Mba \* 

Dipartimento di Scienze Chimiche, Università degli Studi di Padova, Via Marzolo 1, 35131 Padova, Italy

\* Correspondence: miriam.mba@unipd.it

**Abstract:** The conjugation of small-molecule semiconductors with self-assembling peptides is a powerful tool for the fabrication of supramolecular soft materials for organic electronics and bioelectronics. Herein, we introduced the benchmark organic semiconductor [1]benzothieno[3,2-b][1]-benzothiophene (BTBT) within the structure of a self-assembling amphiphatic peptide. The molecular structure of the conjugate was rationally designed to favour  $\pi$ - $\pi$  stacking between BTBT cores and  $\pi$ -delocalization within the self-assembled architectures. Hydrogels with fibrillar structure were obtained upon self-assembly. Spectroscopic studies confirmed that both hydrogen bonding between peptide segments and  $\pi$ - $\pi$  stacking between BTBT chromophores are responsible for the formation of the 3D fibrillar network observed by transmission electron microscopy. The hydrogel was successfully deposited on gold interdigitated electrodes and a conductivity up to  $1.6 (\pm 0.1) \times 10^{-5} \text{ S cm}^{-1}$  was measured.

**Keywords:** [1]benzothieno[3,2-b][1]-benzothiophene; peptide; supramolecular hydrogel; peptide-chromophore conjugate;  $\pi$ -gel; electrically conductive hydrogel



**Citation:** Fortunato, A.; Hensel, R.C.; Casalini, S.; Mba, M. Self-Assembly and Electrical Conductivity of a New [1]benzothieno[3,2-b][1]-benzothiophene (BTBT)-Peptide Hydrogel. *Molecules* **2023**, *28*, 2917. <https://doi.org/10.3390/molecules28072917>

Academic Editors: Francesca Iemma, Manuela Curcio and Alessia Irrera

Received: 28 February 2023

Revised: 22 March 2023

Accepted: 22 March 2023

Published: 24 March 2023



**Copyright:** © 2023 by the authors. Licensee MDPI, Basel, Switzerland. This article is an open access article distributed under the terms and conditions of the Creative Commons Attribution (CC BY) license (<https://creativecommons.org/licenses/by/4.0/>).

## 1. Introduction

Molecular self-assembly of small  $\pi$ -conjugated molecules (SCM) with optoelectronic properties is a powerful tool for the fabrication of feasible ordered nanoarchitectures for organic electronics [1,2]. In this context, the self-assembly of oligothiophenes [3] or p-phenylenevinylenes [4] has been explored extensively in the literature.

In a common approach, the functionalization of the SCM with a specific self-assembling unit introduces additional non-covalent interactions and allows control over the supramolecular organisation. This approach leads to a robust and well-ordered supramolecular architecture in which the SCMs have specific positions, which in turn may affect the efficiency of electronic coupling. Due to its biocompatibility and ability to undergo self-assembly, the conjugation of biomolecules to SCM has been suggested as a powerful approach [5]. Among the various biomolecules capable of self-assembly into ordered supramolecular architectures [6,7], peptides [8], in particular short peptides [9], stand out for several reasons. Peptides are known to form well-ordered secondary structures through directional hydrogen bonds, and their self-assembling properties can be tuned by a proper selection of the amino acid sequence. For example, sequences that feature an alternation of hydrophilic and hydrophobic amino acids are known to favour the formation of 1D  $\beta$ -sheet structures [10,11]. Furthermore, peptides can be easily synthesised with a plethora of available natural and non-natural amino acids. In addition, they also offer biocompatibility [12,13] and the possibility of aqueous processing of the material [14]. In this context, supramolecular peptide hydrogels have been of particular interest in recent years [15–17]. Peptides self-assemble in water to give a 3D fibrillar network that entraps the solvent, yielding a gel. Thus, hydrogelation is a process that easily allows the fabrication of 1D supramolecular structures and soft materials for organic electronics [18]. Hydrogelation

of peptide conjugates has been used successfully to obtain soft materials incorporating different SCM such as pyrene [19,20], oligothiophenes [21], naphthalene diimide [22], oligo-para(phenylenevinylene) [23], or diketopyrrolopyrrole [24].

Among SCMs, [1]benzothieno[3,2-b][1]benzothiophene (BTBT) is a promising small-molecule p-type semiconductor [25,26]. Soluble dialkyl, monoalkyl and aryl derivatives allow for solution processes and combine solubility and high hole mobility featuring good thermal stability [27–30]. For example, Yuan et al. reported an impressive thin film transistor hole mobility of  $43 \text{ cm}^2 \text{ V}^{-1} \text{ s}^{-1}$  for the 2,7-dioctyl-substituted BTBT (C8-BTBT) [31]. Despite these important achievements, the development of water-processable and biocompatible BTBT derivatives remains an open challenge. Guler et al. were the first to report two amphiphilic BTBT peptide conjugates, in which BTBT was introduced at the N-terminus separated from the peptide sequence by a flexible linker [32]. These hybrid molecules self-assembled in water to form nanofibers that showed an average conductivity of  $4.2 (\pm 1.8) \times 10^{-6} \text{ S cm}^{-1}$  and  $2.4 (\pm 0.47) \times 10^{-7} \text{ S cm}^{-1}$  for the BTBT-peptide and the C8-BTBT-peptide, respectively. More recently, we reported the first BTBT-peptide hydrogel [33]. We functionalised the N-terminus of a  $\beta$ -sheet self-assembling tetrapeptide containing glutamic acid (Glu) and phenylalanine (Phe), namely Glu-Phe-Glu-Phe, with the BTBT core. Furthermore, hydrogels were obtained by tuning both the pH and the ionic strength of the solution.

As mentioned above, the type of amino acids and their sequence determine the type of self-assembly, and thus, subtle structural variations might lead to changes in the type and strength of the non-covalent interactions involved, also leading to different supramolecular architectures [34–36]. For this reason, we aimed to study the effect of introducing the BTBT core in the side chain of the main peptide backbone. To favour a straightforward synthesis of this derivative, the Cu(I)-catalysed azido alkyne cycloaddition (CuAAC) was used to functionalise the amino acid side chain with the BTBT core. An alternating sequence of hydrophilic and hydrophobic amino acids was maintained in order to favour  $\beta$ -sheet formation. Self-supporting transparent hydrogels were obtained upon pH switching. We investigated the solution-based thin film deposition and the electrical properties of this new material.

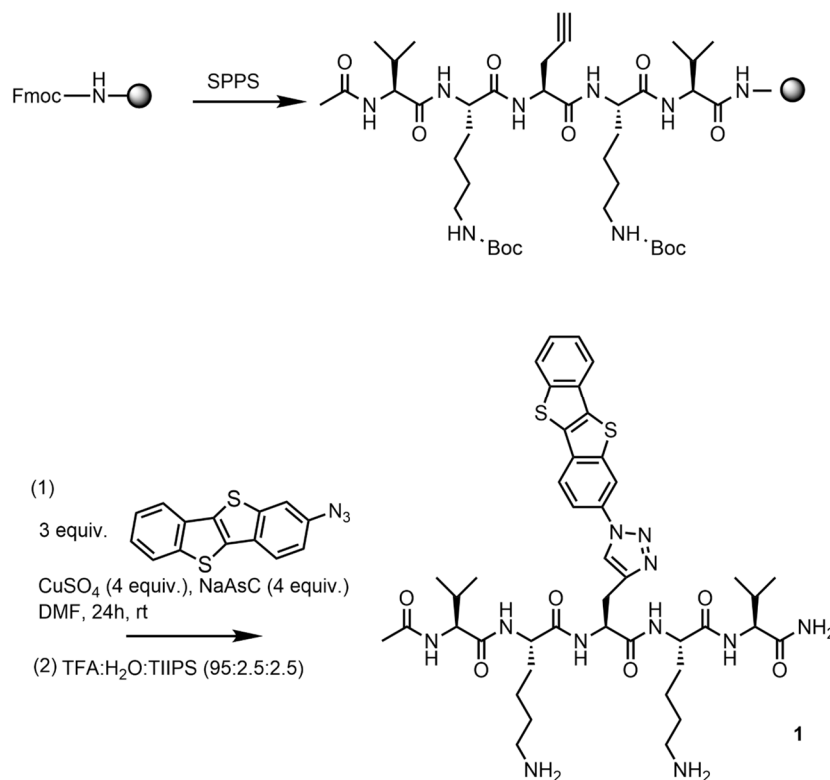
## 2. Results and Discussion

### 2.1. Design and Synthesis of the BTBT-Peptide Hybrid 1

The molecular architecture of the BTBT-peptide hybrid **1** (Scheme 1) alternates hydrophilic and hydrophobic residues in its structure. This alternation favours the formation of  $\beta$ -sheet structures in which the side chains of adjacent residues point out in opposite directions, generating two distinct faces: a hydrophobic and a hydrophilic one. In aqueous media, two sheets may self-assemble to form a  $\beta$ -sheet bilayer in which hydrophobic residues are buried inside, while the hydrophilic faces are exposed to the solvent. It has been demonstrated that this type of self-assembly can accommodate large aromatic side-chains in the inner shielded region and that increasing the area of the aromatic surface leads to stronger  $\pi$ - $\pi$  interactions [37]. Thus, we expected to obtain self-assembled nanostructures with an aromatic core in which strong  $\pi$ - $\pi$  interactions are established between BTBT chromophores.

Concerning the peptide design, two valine residues (Val) were positioned at the N- and C-termini, the hydrophilic lysine residues (Lys) enabled pH-dependent solubility in water, while the central position was occupied by the non-natural amino acid L-propargylglycine (Pra) functionalised with BTBT. The N-acetylated peptide sequence was synthesised following fluorenylmethoxycarbonyl (Fmoc) solid-phase peptide synthesis (SPPS) protocols on a 4-methylbenzhydrylamine (MHBA) Rink amide resin. Couplings were carried out using a mixture of O-benzotriazole-N,N,N',N'-tetramethyluronium hexafluorophosphate (HBTU), 1-Hydroxybenzotriazole hydrate (HOBt), and N,N-diisopropylethylamine (DIPEA). Fmoc deprotection was achieved by treatment with a 20% solution of 4-methylpiperidine in dimethylformamide (DMF). The BTBT moiety was then introduced through an on-resin

CuAAC reaction between the terminal alkyne of the Pra side chain and the azide group of 2-azido-BTBT (**2**) in the presence of sodium ascorbate (NaAsc) and  $\text{CuSO}_4$  (Scheme 1). Final cleavage was performed using a trifluoroacetic acid (TFA)/triisopropylsilane (TIPS)/water cocktail (See Supporting Information for details). Compounds **1** and **2** were thoroughly characterised by NMR, FT-IR and ESI-MS (See Figures S1–S8 of the Supporting Information).



**Scheme 1.** Synthesis of the BTBT-peptide conjugate **1**.

## 2.2. Gelation and Hydrogel Characterization

**1** is well soluble in acidic water, where the Lys side chains are protonated. When the pH of the solution was raised above 10 by adding NaOH 0.5 N, a self-supporting hydrogel was formed in a few minutes (Figure 1a). The minimum gelation concentration (mgc) was equal to 0.5 wt % and the gel-to-solution transition ( $T_{\text{gel}}$ ) was observed at 80 °C.

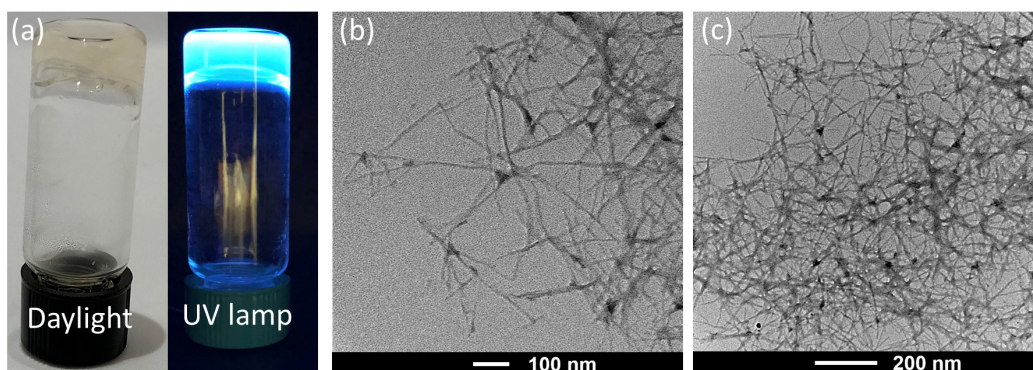


**Figure 1.** (a) Photograph of the gel under daylight and UV lamp; gel formation was assessed by the vial inversion test. (b,c) TEM micrographs of the xerogels.

The morphology of the self-assembled nanostructures was analysed by transmission electron microscopy (TEM). TEM micrographs of the xerogel revealed the formation of

long-range fibres with an average diameter of 10 ( $\pm 2$ ) nm and a length of up to 500 nm (Figure 1b,c).

The gel nature of the sample was confirmed via oscillatory rheology. As expected for viscoelastic materials, frequency sweep experiments showed that the elastic modulus ( $G'$ ) was one order of magnitude higher than the viscous one ( $G''$ ) within the linear viscoelastic region, and both contributions were frequency-independent within the investigated range (Figure 2a). In the strain sweep set-up, the viscous and elastic modulus deviated from linearity above 3% of applied strain, reaching the cross-over point at 25% of strain (Figure 2b).

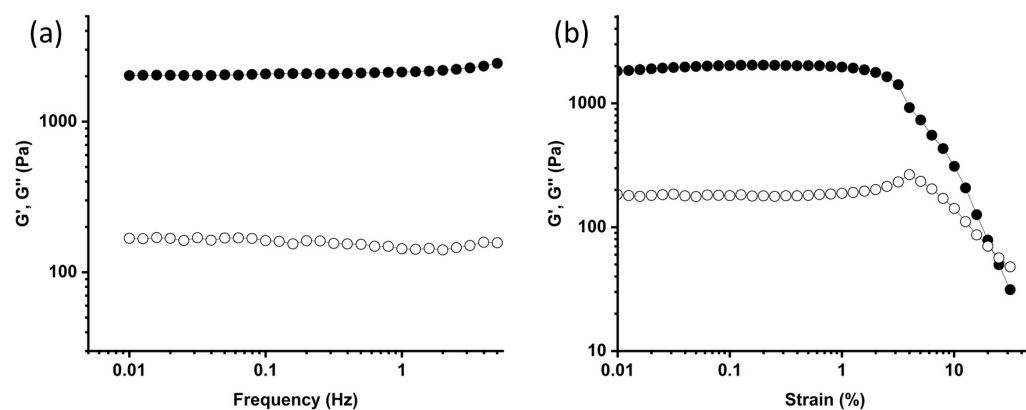


**Figure 2.** (a) Frequency sweep experiment and (b) strain sweep experiment of gel at 0.5 wt % concentration; filled circles represent  $G'$  while open circles represent  $G''$ .

Self-assembly was also investigated by UV-Vis absorption and emission spectroscopies and circular dichroism (CD).

The UV-Vis absorption spectrum of a  $10^{-5}$  M solution of **1** in MilliQ water showed a structured band going from 285 nm to 350 nm originating from the BTBT core (Figure 3a) [38]. The absorption maximum was centred at 315 nm, with a shoulder located at 340 nm. The emission profile was characterised by an asymmetric band centred at 415 nm with a less-pronounced shoulder at 430 nm. Increasing the concentration to 0.5 wt % ( $5.6 \times 10^{-3}$  M), a widening of the absorption band of about 12 nm was observed. The maximum absorption peak remained at 315 nm while the less-pronounced shoulder red-shifted to 352 nm. Even the emission spectroscopy showed a broadening of the profile (Figure 3b). The broad emission band showed a maximum at 415 nm, with a shoulder at 440 nm and a long tail up to 620 nm. In an alkaline environment (viz. pH > 10), the gel was formed. The pH-triggered hydrogel showed the broadest UV-Vis absorption spectrum. The main absorption band ranged from 305 nm to 340 nm, while the shoulder increased its intensity and moved to 355 nm. The emission maximum was red-shifted to 445 nm and a tail was observed up to 650 nm.

These data suggest the presence of strong  $\pi$ - $\pi$  interactions between the BTBT chromophores upon gelation.

This hypothesis was confirmed by CD investigations (Figure 3c). The CD spectrum of a  $10^{-5}$  M solution of **1** in water showed a silent CD in the BTBT absorption region and a negative peak at 200 nm that indicates a random coil conformation of the peptide segment. Upon increasing the concentration, new strong negative CD signals emerge at 228 nm and above 280 nm, in the BTBT absorption region, suggesting the formation of  $\beta$ -sheet structures [39] and a chiral arrangement of the chromophores within the aggregate. In the hydrogel, the intensity of the CD signal decreased significantly as a consequence of scattering due to the formation of the 3D fibrillar network. Nevertheless, five negative peaks, located at 368 nm, 332 nm, 320 nm, 280 nm, and 220 nm, could be detected. Signals above 280 nm arise from the BTBT moiety, indicating that the chromophore is involved

in the formation of a chiral structure. The negative peak at 220 nm is consistent with the formation of a H-bonded  $\beta$ -sheet network [39].

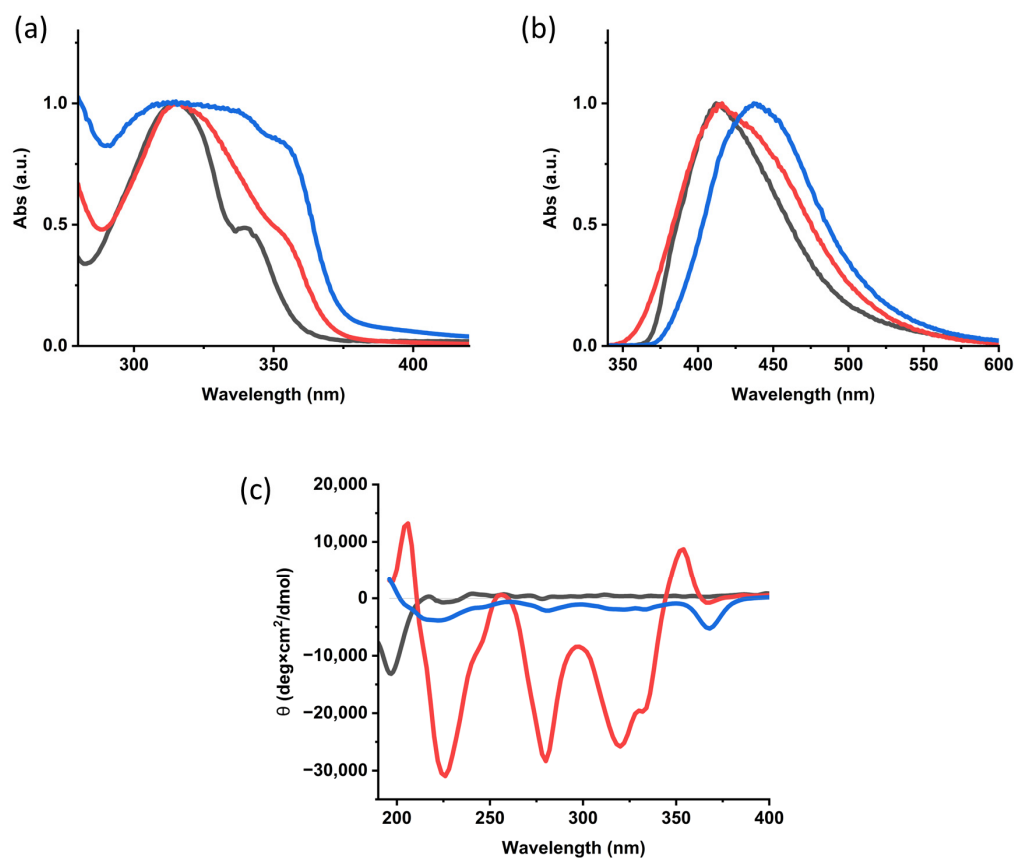


**Figure 3.** Normalized (a) UV-Vis absorption and (b) emission spectra and (c) CD spectra of **1** in aqueous solution at  $10^{-5}$  M (black line), at  $5.6 \times 10^{-3}$  M (red line) and the gelled sample (blue line).

### 2.3. Electrical Characterization

In recent years, 2D and 3D conductive hydrogel scaffolds have been extensively studied due to their potential use in tissue engineering applications [40]. We evaluated the charge-transport behaviour of the designed gelator by performing electrical measurements on drop-casted thin films deposited on gold interdigitated electrodes. The hydrogels were first obtained at the mgc concentration and then diluted with water immediately prior to deposition (Figure 4). Optimization of the deposition process showed that the addition of 1% *v/v* of N-methyl-2-pyrrolidone (NMP) is necessary to avoid the formation of a “coffee ring” [41]. The addition of NMP did not affect the spatial organisation of the gelator, and the fibrillar structure was maintained, as confirmed by SEM micrographs (Figure S9 of the Supporting Information). Upon drop-casting, the sample was dried at room temperature and then kept under a primary vacuum overnight. Interestingly, we noted that the outcome of the deposition was highly affected by its surrounding. To ensure the reproducibility of the deposition, it was necessary to maintain the NMP-water reservoir close to the BTBT droplets to regulate humidity and allow a control over the drying process. In this context, a few droplets of the 1% NMP solution were placed on the Si/SiO<sub>2</sub> substrates prior to the deposition of BTBT.

This specific deposition allowed the control and formation on top of the electrodes of dendrimeric features, as shown in Figure 5a–c. These particular structures were able to electrically bridge the interdigitated electrodes. These fibrillar structures are physically adsorbed, hence they can be completely removed by rinsing the substrate with water (Figure 5c,d).

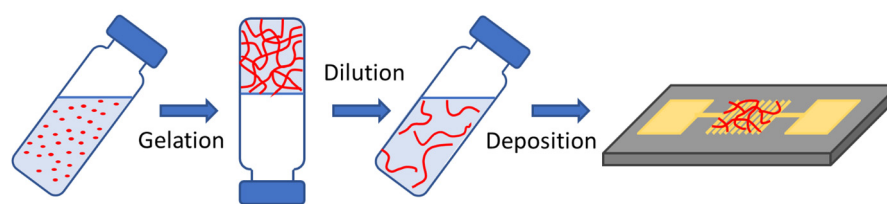


**Figure 4.** Schematic representation of the deposition process.

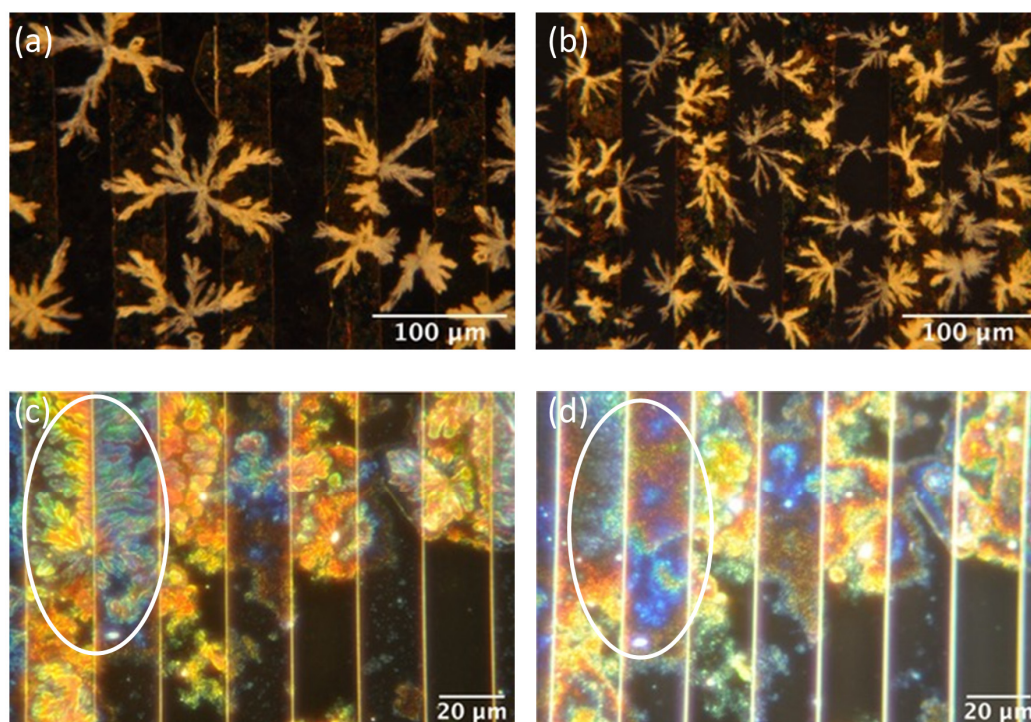


**Figure 5.** Dark-field optical microscope images of **1** deposited on gold interdigitated electrodes (a,b). (c,d) Dark-field optical microscope images before and after rising with water, respectively. White circle highlights the removal of adsorbed dendrimeric shapes.

Electrical characterisation was performed by recording the I-V characteristics of the BTBT devices in the air. Figure 6a,b present the I-V profile obtained when the voltage was swept from 0 V to +1 V, and from −3 V to +3 V, respectively. In Figure 6a, it is possible to observe a rectifying behaviour due to the p-n diodes composed by the Au electrode and the BTBT film [32]. This trend is ruled by Equation (1):

$$I = I_0 \left[ \exp\left(\frac{V}{A}\right) - 1 \right], \quad (1)$$

in which  $I_0$  corresponds to the reverse bias current, and  $A$  is a linear function of the ideality factor and the thermal voltage. Within this context, the first derivative of current with respect to the applied voltage indicates a diode-limited current that evolves to a resistor-limited current when the applied voltage approaches 1 V. In the resistive region, the linear fit provides a conductivity of  $5.3 (\pm 0.1) \times 10^{-7} \text{ S cm}^{-1}$ , which has the same order of magnitude as that presented in the literature for C8-BTBT-peptide films. Nevertheless, as our device works in a voltage range that is twenty times lower, it opens up the possibility of being applied on low-power devices. We also investigated the electrical response of the BTBT devices in a broader voltage range, as shown in Figure 6b. In this case, a peak was observed at +1.3 V and −1.2 V. Such a feature has already been reported in the literature for the cyclic voltammetry of BTBT in 1 mM dichloromethane, and it was attributed to reversible

redox of the BTBT compounds [42]. However, as our measurements are performed in the air, we attribute the presence of such redox activity to the presence of trapped water in the BTBT compound, which allows for charge transport. The superposition of these peaks to the diode profile causes a reduction in the measured current in the resistive region according to consecutive scans. The stability of these devices was achieved by leaving the samples in vacuum overnight and by shielding them with a drop-casted PMMA layer. The PMMA layer also prevented the detachment of dendrimeric features from the substrate. Figure S10 of the Supporting Information illustrates the improved performance for six consecutive scans. Under these conditions, the resistive region provides a conductivity of  $1.6 (\pm 0.1) \times 10^{-5} \text{ S cm}^{-1}$ . This value is one order of magnitude higher than the conductivity reported previously for other non-gelled assemblies of BTBT-peptide hybrids [32].

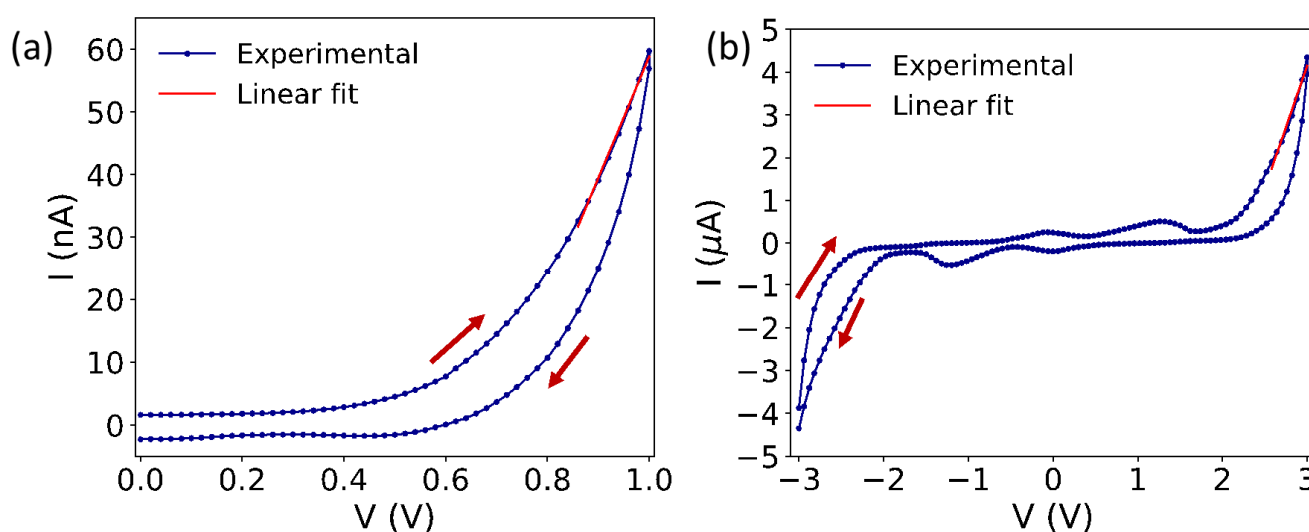


**Figure 6.** I-V plots of the BTBT onto Au IDEs in which the applied voltage swept from (a) 0 V to +1 V, and (b) −3 V to +3 V.

### 3. Materials and Methods

**Preparative high performance liquid chromatography (HPLC):** This was performed using an ÄKTA Pure GE Healthcare apparatus equipped with a Jupiter C18 (250 × 22 mm, 10 μm, 300 Å) column. The UV SPD-20A detector was used at 217 nm, flow rate 15 mL/min, in a binary elution system (solvent A: H<sub>2</sub>O + 0.05% TFA; solvent B: acetonitrile + 0.05% TFA).

**Analytical HPLC-MS:** HPLC-MS analysis was performed by using an HPLC Agilent Technologies 1260 Infinity II equipped with a KINETEX XB C18 (100 × 4.60 mm, 100 Å, 3.5 μm) column. HPLC was connected with an Agilent Technologies 6130 Quadrupole LC/MS instrument. Solvent A: H<sub>2</sub>O + 0.05% TFA; solvent B: ACN + 0.05% TFA.

**Nuclear Magnetic Resonance (NMR):** <sup>1</sup>H and <sup>13</sup>C NMR spectra were collected at room temperature on Bruker Avance II 300 or Bruker 400 spectrometers. Chemical shifts (δ) were reported in parts per million (ppm). The signal of the partially deuterated solvent was used as internal standard. The signal multiplicity was indicated as s (singlet), d (doublet), t (triplet), m (multiplet), and br (broad).

**Fourier Transform Infrared Spectroscopy (FT-IR):** FT-IR spectra were recorded using a Perkin-Elmer 720× spectrophotometer at a nominal resolution of 2 cm<sup>−1</sup> with an average scan of 100.

**UV-Vis absorption spectroscopy:** UV-Vis absorption spectra were registered using a Varian Cary 50 spectrophotometer at room temperature in a baseline correction mode. Rectangular cells with an optical path of 10 mm or 1 mm were used for the diluted and concentrated solution, respectively. For gelled samples, a detachable window cell with

0.2 mm optical path was employed. All gels were previously prepared in a vial and then transferred to the quartz chamber, which was carefully closed to avoid the formation of bubbles.

**Emission spectroscopy:** Emission spectra were registered using a Varian CaryE-clipse spectrophotometer at room temperature. Rectangular cells with an optical path of  $10 \times 10$  mm were used for diluted solutions, while concentrated solutions and gels were analysed using a cell with a  $10 \times 4$  mm optical path. For gelled samples, the gel was directly prepared within the quartz cell and analysed without amendment.

**Circular Dichroism (CD) Spectroscopy:** CD spectra were collected using a Jasco J-1500 spectropolarimeter at room temperature, as an average of 32 measurements. Baselines were recorded for all spectra. Spectra were reported in terms of total molar ellipticity ( $\text{deg} \times \text{cm}^2 \times \text{dmol}^{-1}$ ). The diluted solutions were analysed using a cuvette cell of 10 mm path length, while concentrated solutions were analysed in a 1 mm path length cuvette. Gelled samples were previously prepared in a glass vial and then transferred to a cell with detachable windows and an optical path of 0.2 mm without amendment, and avoiding bubble formation.

**Transmission Electron Microscopy (TEM):** TEM analysis was performed using a Jeol 300PX TEM instrument. Glow-discharged carbon-coated grids were used. The grid was floated on a small drop of the sample and the excess was removed by Whatman filter paper, grade 50, hardened. Gels were diluted prior to the analysis. The micrographs were analysed using the ImageJ program.

**Rheology:** Rheological investigations were performed on a Kinexus Lab+ rheometer at room temperature with an anti-evaporation chamber to prevent sample dryness. Gels were prepared in a mould with 2 cm diameter and transferred onto the plate immediately before the analysis. Two-parallel-plated geometry was used for the analysis. Frequency sweep experiments were carried out between 5 Hz and 0.001 Hz at a constant 0.2% strain. Strain sweep experiments were carried out at a constant frequency of 0.2 Hz, varying the strain between 0.01% and 100%.

**Electrical measurements:** Gold interdigitated electrodes (IDEs), deposited on Si/SiO<sub>2</sub> and composed of 11 digits having 733  $\mu\text{m}$  length, 40  $\mu\text{m}$  width, and spaced 40  $\mu\text{m}$  from each other (cell constant  $\approx 3665 \mu\text{m}$ ), were produced by standard photolithography and used for the electrical characterizations. Samples of 1 mg/mL jellified BTBT were dispersed in bi-distilled water at a concentration of 0.2 mL/mL. The obtained dispersion was then drop-casted onto the IDEs in a 1% NMP atmosphere. The dried samples were put in a vacuum overnight and covered by the drop-casting deposition of 5% PMMA in anisole ( $w/v$ ). Electrical characterizations were performed in a Faraday cage in the air and in the dark. An Agilent B1500 parameter analyser equipped with two high-power and two high-resolution source measurement units (SMUs) was used for the I-V characterization.

**Synthesis of compound 1:** 1 was achieved using standard SPPS protocols followed by CuCAAC reaction and peptide cleavage (Details can be found in the Supporting Information). **On-resin CuAAC reaction:** The resin was transferred into a vial and a solution of 2 (3 equiv.) in degassed DMF (10 mL per 1 g of resin) was added, followed by CuSO<sub>4</sub> (4 equiv.), L-sodium ascorbate (NaAsc, 4 equiv.) and DIPEA (9 equiv.). The mixture was shaken for 24 h at room temperature and the reaction was monitored via HPLC. When the reaction was completed, the mixture was transferred to an SPPS reaction vessel and the resin was washed with DMF ( $\times 6$ ), H<sub>2</sub>O ( $\times 6$ ), Ethylenediaminetetraacetic acid (EDTA, 0.1 M, pH = 6,  $\times 5$ ), H<sub>2</sub>O ( $\times 6$ ), and DMF ( $\times 6$ ). <sup>1</sup>H-NMR (400 MHz, DMSO-d<sub>6</sub>)  $\delta$  (ppm), 8.748 (d,  $J = 2.0$  Hz, 1H), 8.625 (s, 1H), 8.291 (d,  $J = 8.6$  Hz, 1H), 8.240 (d,  $J = 7.3$  Hz, 1H), 8.205 (d,  $J = 7.2$  Hz, 1H), 8.147–8.094 (m, 3H), 8.074 (dd,  $J = 8.6, 2.0$  Hz, 1H), 7.831 (d,  $J = 8.2$  Hz, 1H), 7.804–7.706 (m, 7H), 7.609–7.490 (m, 2H), 7.415 (s, 1H), 7.081 (s, 1H), 4.634 (q,  $J = 7.3$  Hz, 1H), 4.294 (d,  $J = 6.7$  Hz, 1H), 4.254–4.023 (m, 3H), 3.234 (dd,  $J = 15.1, 5.2$  Hz, 1H), 3.070 (dd,  $J = 15.1, 8.3$  Hz, 1H), 2.813–2.690 (m, 4H), 2.035–1.798 (m, 1H), 1.865 (s, 3H), 1.773–1.457 (m, 8H), 1.400–1.240 (m, 4H), 0.887–0.730 (m, 12H). <sup>13</sup>C NMR (100 MHz, DMSO-d<sub>6</sub>)  $\delta$  (ppm), 172.80, 171.54, 171.48, 171.31, 170.41, 169.59, 144.23, 142.65, 141.85, 134.26, 134.08, 132.36,

132.19, 132.06, 125.94, 125.59, 124.64, 122.85, 121.92, 121.36, 117.85, 115.79, 58.10, 57.51, 52.74, 52.62, 52.05, 38.64, 31.16, 30.83, 30.45, 30.14, 26.61, 26.52, 22.49, 22.27, 22.20, 19.24, 19.19, 18.21, 17.91. ESI-MS:  $[M+H]^+$  calculated for  $C_{43}H_{59}N_{11}O_6S_2$  890.14, found 890.5.  $[M+Na]^+$  calculated for  $C_{43}H_{59}N_{11}O_6S_2$  912.14, found 912.5. FT-IR (KBr):  $\nu(\text{cm}^{-1}) = 3407, 3285, 3074, 2963, 2932, 2664, 1674, 1628, 1527, 1430, 1340, 1300, 1243, 1200, 1180, 1132, 1041, 992, 950, 838, 798, 748, 721, 703, 600$ .

Synthesis of **2**: 2-amino-[1]benzothieno[3,2-b][1]benzothiophene [43] (1.2 g, 4.73 mmol), previously ground, was dispersed in HCl 6 M (27 mL) and heated at 70 °C for 20 min. The reaction mixture was cooled to room temperature and then to 0 °C by using an ice/water bath. A cooled aqueous solution of  $\text{NaNO}_2$  (420 mg, 6.08 mmol in 12.6 mL MilliQ water) was added dropwise. The suspension was stirred for 30 min at 0 °C. Next, the reaction mixture was added dropwise to a solution of  $\text{NaN}_3$  (426 mg, 6.55 mmol in 12.6 mL MilliQ water) cooled to 0 °C. The mixture was stirred at the same temperature for 2 h, then the aqueous phase was extracted with dichloromethane (DCM) (3×), washed with water and brine, dried over  $\text{NaSO}_4$ , and filtered and evaporated to give a brownish solid that was used in the next step without further purification (yield 76%).  $^1\text{H}$  NMR (300 MHz,  $\text{DMSO-d}_6$ )  $\delta$  (ppm), 8.22–7.93 (m, 4H), 7.49 (m 2H), 7.26 (dd,  $J = 8.5, 2.1$  Hz, 1H).  $^{13}\text{C}$  NMR (75 MHz,  $\text{DMSO-d}_6$ )  $\delta$  (ppm), 143.24, 141.50, 137.08, 132.72, 132.48, 132.31, 129.68, 125.48, 125.41, 124.47, 122.87, 121.59, 117.38, 114.69. FT-IR:  $\nu(\text{cm}^{-1})$  3431, 2107, 1552, 1465, 1339, 1284, 951, 809, 748.

Gel formation: 5 mg of **1** were dissolved in MilliQ water (900  $\mu\text{L}$ ) with the aid of sonication. The addition of NaOH (0.5 M, 3 equiv.) and MilliQ water allowed the obtaining of a self-supporting hydrogel with the desired final concentration of 5 mg/mL. Gel formation was assessed via a vial inversion test.

#### 4. Conclusions

In summary, we successfully designed and synthesised a hybrid peptide, whose backbone incorporated the [1]benzothieno[3,2-b]benzothiophene (BTBT) small-molecule semiconductor. The hybrid peptide was effectively self-assembled in water to give self-supporting hydrogels upon pH-switching with a fibrillar structure. Spectroscopic studies confirmed the formation of  $\beta$ -sheet assemblies and revealed the presence of strong  $\pi$ - $\pi$  interactions between BTBT cores, that result in  $\pi$ -delocalization. Such hybrid peptides showed high conductivity values, as high as  $5.3 (\pm 0.1) \times 10^{-7} \text{ S cm}^{-1}$ , corresponding to low operational voltages (i.e.,  $0 < V < 1 \text{ V}$ ). Broadening the voltage range ( $-3 \text{ V} < V < +3 \text{ V}$ ), we reached a conductivity value equal to  $1.6 (\pm 0.1) \times 10^{-5} \text{ S cm}^{-1}$ . To the best of our knowledge, this conductivity value is one order of magnitude higher than state-of-the-art values reported in the literature related to non-gel BTBT-peptide hybrids. Such promising results pave the way towards interesting applications, where a soft, nanostructured, electrically-active and biocompatible material is required.

**Supplementary Materials:** The following supporting information can be downloaded at: <https://www.mdpi.com/article/10.3390/molecules28072917/s1>, Detailed synthetic procedures and characterization of **1** and **2** [43]. Figure S1:  $^1\text{H}$  NMR ( $\text{DMSO-d}_6$ , 300 MHz) of **2**, Figure S2:  $^{13}\text{C}$  NMR ( $\text{DMSO-d}_6$ , 75 MHz) of **2**, Figure S3:  $^1\text{H}$  NMR ( $\text{DMSO-d}_6$ , 400 MHz) of **1**, Figure S4:  $^{13}\text{C}$ -NMR ( $\text{DMSO-d}_6$ , 100 MHz) of **1**, Figure S5: FT-IR spectrum of **2** (KBr disk), Figure S6: FT-IR spectrum of **2** (KBr disk), Figure S7: HPLC chromatogram of **1**, Figure S8: ESI-MS of **1**, Figure S9: SEM micrographs of the gel, Figure S10: Consecutive I-V measurements of the BTBT-peptide onto Au IDEs in which the applied voltage swept from  $-3 \text{ V}$  to  $+3 \text{ V}$ .

**Author Contributions:** Author Contributions: Conceptualization, M.M., S.C.; synthesis, A.F.; characterization of organic compounds, A.F. and M.M.; electrical measurements, S.C., R.C.H. and A.F.; writing—original draft preparation, A.F., R.C.H., S.C. and M.M.; writing—review and editing, A.F., R.C.H., S.C. and M.M.; supervision, M.M, S.C. All authors have read and agreed to the published version of the manuscript.

**Funding:** S.C. and R.C.H. acknowledge the funding from the University of Padua, Department of Chemical Sciences (P-DiSC#11NexuS\_BIRD2020-UNIPD-CARBON-FET-) and from the Italian Ministry of Education, Universities and Research (Nanochemistry for Energy and Health, NExuS, within the national funding network termed “Dipartimenti di Eccellenza”).

**Institutional Review Board Statement:** Not applicable.

**Informed Consent Statement:** Not applicable.

**Data Availability Statement:** The data presented in this study are available in the article and/or supplementary material.

**Acknowledgments:** A.F. and M.M. thank Barbara Biondi for providing instrument access and assistance with preparative HPLC.

**Conflicts of Interest:** The authors declare no conflict of interest.

## References

1. Hoeben, F.J.; Jonkheijm, P.; Meijer, E.; Schenning, A.P. About supramolecular assemblies of  $\pi$ -conjugated systems. *Chem. Rev.* **2005**, *105*, 1491–1546. [[CrossRef](#)] [[PubMed](#)]
2. Chen, H.; Fraser Stoddart, J. From molecular to supramolecular electronics. *Nat. Rev. Mater.* **2021**, *6*, 804–828. [[CrossRef](#)]
3. Leclere, P.; Surin, M.; Viville, P.; Lazzaroni, R.; Kilbinger, A.; Henze, O.; Feast, W.; Cavallini, M.; Biscarini, F.; Schenning, A. About oligothiophene self-assembly: From aggregation in solution to solid-state nanostructures. *Chem. Mater.* **2004**, *16*, 4452–4466. [[CrossRef](#)]
4. Ajayaghosh, A.; Praveen, V.K.  $\pi$ -Organogels of self-assembled p-phenylenevinylenes: Soft materials with distinct size, shape, and functions. *Acc. Chem. Res.* **2007**, *40*, 644–656. [[CrossRef](#)]
5. Jatsch, A.; Schillinger, E.-K.; Schmid, S.; Bäuerle, P. Biomolecule assisted self-assembly of  $\pi$ -conjugated oligomers. *J. Mater. Chem.* **2010**, *20*, 3563–3578. [[CrossRef](#)]
6. Gong, C.; Sun, S.; Zhang, Y.; Sun, L.; Su, Z.; Wu, A.; Wei, G. Hierarchical nanomaterials via biomolecular self-assembly and bioinspiration for energy and environmental applications. *Nanoscale* **2019**, *11*, 4147–4182. [[CrossRef](#)] [[PubMed](#)]
7. Wang, L.; Gong, C.; Yuan, X.; Wei, G. Controlling the Self-Assembly of Biomolecules into Functional Nanomaterials through Internal Interactions and External Stimulations: A Review. *Nanomaterials* **2019**, *9*, 285. [[CrossRef](#)]
8. Ekiz, M.S.; Cinar, G.; Khalily, M.A.; Guler, M.O. Self-assembled peptide nanostructures for functional materials. *Nanotechnology* **2016**, *27*, 402002. [[CrossRef](#)]
9. Hu, X.; Liao, M.; Gong, H.; Zhang, L.; Cox, H.; Waigh, T.A.; Lu, J.R. Recent advances in short peptide self-assembly: From rational design to novel applications. *Curr. Opin. Colloid Interface Sci.* **2020**, *45*, 1–13. [[CrossRef](#)]
10. Ulijn, R.V.; Smith, A.M. Designing peptide based nanomaterials. *Chem. Soc. Rev.* **2008**, *37*, 664–675. [[CrossRef](#)]
11. Bowerman, C.J.; Nilsson, B.L. Review self-assembly of amphipathic  $\beta$ -sheet peptides: Insights and applications. *Pept. Sci.* **2012**, *98*, 169–184. [[CrossRef](#)] [[PubMed](#)]
12. Silva, G.A.; Czeisler, C.; Niece, K.L.; Beniash, E.; Harrington, D.A.; Kessler, J.A.; Stupp, S.I. Selective Differentiation of Neural Progenitor Cells by High-Epitope Density Nanofibers. *Science* **2004**, *303*, 1352–1355. [[CrossRef](#)] [[PubMed](#)]
13. Ghosh, G.; Barman, R.; Sarkar, J.; Ghosh, S. pH-Responsive Biocompatible Supramolecular Peptide Hydrogel. *J. Phys. Chem. B* **2019**, *123*, 5909–5915. [[CrossRef](#)] [[PubMed](#)]
14. Eakins, G.L.; Pandey, R.; Wojciechowski, J.P.; Zheng, H.Y.; Webb, J.E.A.; Valéry, C.; Thordarson, P.; Plank, N.O.V.; Gerrard, J.A.; Hodgkiss, J.M. Functional Organic Semiconductors Assembled via Natural Aggregating Peptides. *Adv. Func. Mater.* **2015**, *25*, 5640–5649. [[CrossRef](#)]
15. Fichman, G.; Gazit, E. Self-assembly of short peptides to form hydrogels: Design of building blocks, physical properties and technological applications. *Acta Biomater.* **2014**, *10*, 1671–1682. [[CrossRef](#)]
16. Mondal, S.; Das, S.; Nandi, A.K. A review on recent advances in polymer and peptide hydrogels. *Soft Matter* **2020**, *16*, 1404–1454. [[CrossRef](#)]
17. Dasgupta, A.; Mondal, J.H.; Das, D. Peptide hydrogels. *RSC Adv.* **2013**, *3*, 9117–9149. [[CrossRef](#)]
18. Ardoña, H.A.M.; Tovar, J.D. Peptide  $\pi$ -Electron Conjugates: Organic Electronics for Biology? *Bioconjug. Chem.* **2015**, *26*, 2290–2302. [[CrossRef](#)]
19. Bartocci, S.; Berrocal, J.A.; Guarracino, P.; Grillaud, M.; Franco, L.; Mba, M. Peptide-Driven Charge-Transfer Organogels Built from Synergetic Hydrogen Bonding and Pyrene–Naphthalenediimide Donor–Acceptor Interactions. *Chem. Eur. J.* **2018**, *24*, 2920–2928. [[CrossRef](#)] [[PubMed](#)]
20. Kaur, H.; Roy, S. Enzyme-Induced Supramolecular Order in Pyrene Dipeptide Hydrogels for the Development of an Efficient Energy-Transfer Template. *Biomacromolecules* **2021**, *22*, 2393–2407. [[CrossRef](#)] [[PubMed](#)]
21. Dibble, J.P.; Troyano-Valls, C.; Tovar, J.D. A Tale of Three Hydrophobicities: Impact of Constitutional Isomerism on Nanostructure Evolution and Electronic Communication in  $\pi$ -Conjugated Peptides. *Macromolecules* **2020**, *53*, 7263–7273. [[CrossRef](#)]

22. Shao, H.; Parquette, J.R. A pi-conjugated hydrogel based on an Fmoc-dipeptide naphthalene diimide semiconductor. *Chem. Commun.* **2010**, *46*, 4285–4287. [[CrossRef](#)] [[PubMed](#)]
23. Mba, M.; Moretto, A.; Armelao, L.; Crisma, M.; Toniolo, C.; Maggini, M. Synthesis and self-assembly of oligo(p-phenylenevinylene) peptide conjugates in water. *Chem. Eur. J.* **2011**, *17*, 2044–2047. [[CrossRef](#)] [[PubMed](#)]
24. Rani, A.; Kaviani, I.; Hume, P.; De Leon-Rodriguez, L.M.; Kihara, S.; Williams, D.E.; McGillivray, D.J.; Plank, N.O.; Gerrard, J.; Hodgkiss, J.M. Directed self-assembly of peptide–diketopyrrolopyrrole conjugates—a platform for bio-organic thin film preparation. *Soft Matter* **2020**, *16*, 6563–6571. [[CrossRef](#)]
25. Xie, P.; Liu, T.; Sun, J.; Yang, J. Structures, Properties, and Device Applications for [1]Benzothieno[3,2-b] Benzothiophene Derivatives. *Adv. Funct. Mater.* **2022**, *32*, 2200843. [[CrossRef](#)]
26. Takimiya, K.; Osaka, I.; Mori, T.; Nakano, M. Organic semiconductors based on [1]benzothieno[3,2-b][1] benzothiophene substructure. *Acc. Chem. Res.* **2014**, *47*, 1493–1502. [[CrossRef](#)]
27. Ebata, H.; Izawa, T.; Miyazaki, E.; Takimiya, K.; Ikeda, M.; Kuwabara, H.; Yui, T. Highly soluble [1]benzothieno[3, 2-b] benzothiophene (BTBT) derivatives for high-performance, solution-processed organic field-effect transistors. *J. Am. Chem. Soc.* **2007**, *129*, 15732–15733. [[CrossRef](#)]
28. Mori, T.; Nishimura, T.; Yamamoto, T.; Doi, I.; Miyazaki, E.; Osaka, I.; Takimiya, K. Consecutive thiophene-annulation approach to pi-extended thienoacene-based organic semiconductors with [1]benzothieno[3,2-b][1]benzothiophene (BTBT) substructure. *J. Am. Chem. Soc.* **2013**, *135*, 13900–13913. [[CrossRef](#)]
29. Minemawari, H.; Tanaka, M.; Tsuzuki, S.; Inoue, S.; Yamada, T.; Kumai, R.; Shimoi, Y.; Hasegawa, T. Enhanced layered-herringbone packing due to long alkyl chain substitution in solution-processable organic semiconductors. *Chem. Mater.* **2017**, *29*, 1245–1254. [[CrossRef](#)]
30. Niimi, K.; Shinamura, S.; Osaka, I.; Miyazaki, E.; Takimiya, K. Dianthra[2,3-b:2',3'-f]thieno[3,2-b]thiophene (DATT): Synthesis, characterization, and FET characteristics of new pi-extended heteroarene with eight fused aromatic rings. *J. Am. Chem. Soc.* **2011**, *133*, 8732–8739. [[CrossRef](#)]
31. Yuan, Y.; Giri, G.; Ayzner, A.L.; Zoombelt, A.P.; Mannsfeld, S.C.; Chen, J.; Nordlund, D.; Toney, M.F.; Huang, J.; Bao, Z. Ultra-high mobility transparent organic thin film transistors grown by an off-centre spin-coating method. *Nat. Commun.* **2014**, *5*, 3005. [[CrossRef](#)] [[PubMed](#)]
32. Khalily, M.A.; Usta, H.; Ozdemir, M.; Bakan, G.; Dikecoglu, F.B.; Edwards-Gayle, C.; Hutchinson, J.A.; Hamley, I.W.; Dana, A.; Guler, M.O. The design and fabrication of supramolecular semiconductor nanowires formed by benzothienobenzothiophene (BTBT)-conjugated peptides. *Nanoscale* **2018**, *10*, 9987–9995. [[CrossRef](#)] [[PubMed](#)]
33. Fortunato, A.; Sanzone, A.; Mattiello, S.; Beverina, L.; Mba, M. The pH-and salt-controlled self-assembly of [1]benzothieno[3,2-b][1]-benzothiophene–peptide conjugates in supramolecular hydrogels. *New J. Chem.* **2021**, *45*, 13389–13398. [[CrossRef](#)]
34. Ardoña, H.A.M.; Besar, K.; Togninalli, M.; Katz, H.E.; Tovar, J.D. Sequence-dependent mechanical, photophysical and electrical properties of pi-conjugated peptide hydrogelators. *J. Mater. Chem. C* **2015**, *3*, 6505–6514. [[CrossRef](#)]
35. Lehrman, J.A.; Cui, H.; Tsai, W.-W.; Moyer, T.J.; Stupp, S.I. Supramolecular control of self-assembling terthiophene–peptide conjugates through the amino acid side chain. *Chem. Commun.* **2012**, *48*, 9711–9713. [[CrossRef](#)]
36. Jira, E.R.; Shmilovich, K.; Kale, T.S.; Ferguson, A.; Tovar, J.D.; Schroeder, C.M. Effect of Core Oligomer Length on the Phase Behavior and Assembly of pi-Conjugated Peptides. *ACS Appl. Mater. Interfaces* **2020**, *12*, 20722–20732. [[CrossRef](#)]
37. Jones, C.W.; Morales, C.G.; Eltiste, S.L.; Yanchik-Slade, F.E.; Lee, N.R.; Nilsson, B.L. Capacity for increased surface area in the hydrophobic core of  $\beta$ -sheet peptide bilayer nanoribbons. *J. Pept. Sci.* **2021**, *27*, e3334. [[CrossRef](#)]
38. Yilmaz, M.; Ozdemir, M.; Erdogan, H.; Tamer, U.; Sen, U.; Facchetti, A.; Usta, H.; Demirel, G. Micro-/Nanostructured Highly Crystalline Organic Semiconductor Films for Surface-Enhanced Raman Spectroscopy Applications. *Adv. Funct. Mater.* **2015**, *25*, 5669–5676. [[CrossRef](#)]
39. Greenfield, N.J. Using circular dichroism spectra to estimate protein secondary structure. *Nat. Protoc.* **2006**, *1*, 2876–2890. [[CrossRef](#)]
40. Sikorski, P. Electroconductive scaffolds for tissue engineering applications. *Biomater. Sci.* **2020**, *8*, 5583–5588. [[CrossRef](#)]
41. Chow, E.; Herrmann, J.; Barton, C.S.; Raguse, B.; Wiczorek, L. Inkjet-printed gold nanoparticle chemiresistors: Influence of film morphology and ionic strength on the detection of organics dissolved in aqueous solution. *Anal. Chim. Acta* **2009**, *632*, 135–142. [[CrossRef](#)] [[PubMed](#)]
42. Dong, Y.; Li, H.; Liu, J.; Zhang, J.; Shi, X.; Shi, Y.; Li, C.; Liu, Z.; Li, T.; Jiang, L. Asymmetrical [1]Benzothieno [3,2-b][1] benzothiophene (BTBT) derivatives for organic thin-film and single-crystal transistors. *Org. Electr.* **2020**, *77*, 105537. [[CrossRef](#)]
43. Kořata, B.; Kozmík, V.; Svoboda, J. Reactivity of [1]Benzothieno[3,2-b][1]benzothiophene—Electrophilic and Metallation Reactions. *Collect. Czech. Chem. Commun.* **2002**, *67*, 645–664. [[CrossRef](#)]

**Disclaimer/Publisher's Note:** The statements, opinions and data contained in all publications are solely those of the individual author(s) and contributor(s) and not of MDPI and/or the editor(s). MDPI and/or the editor(s) disclaim responsibility for any injury to people or property resulting from any ideas, methods, instructions or products referred to in the content.